metals

MDPI

Review

WC-Based Cemented Carbides with High Entropy Alloyed Binders: A Review

Boris Straumal [1,*] and Igor Konyashin [2]

[1] Osipyan Institute of Solid State Physics of the Russian Academy of Sciences, Ac. Osipyan Str. 2, 142432 Chernogolovka, Russia
[2] Element Six GmbH, Staedeweg 18-24, 36151 Burghaun, Germany
* Correspondence: straumal@issp.ac.ru; Tel.: +7-916-6768673

Abstract: Cemented carbides have belonged to the most important engineering materials since their invention in the 1920s. Commonly, they consist of hard WC grains embedded in a cobalt-based ductile binder. Recently, attempts have been made to substitute the cobalt using multicomponent alloys without a principal component (also known as high entropy alloys—HEAs). HEAs usually contain at least five components in more or less equal amounts. The substitution of a cobalt binder with HEAs can lead to the refinement of WC grains; it increases the hardness, fracture toughness, corrosion resistance and oxidation resistance of cemented carbides. For example, a hardness of 2358 HV, fracture toughness of 12.1 MPa.m$^{1/2}$ and compression strength of 5420 MPa were reached for a WC-based cemented carbide with 20 wt.% of the equimolar AlFeCoNiCrTi HEA with a bcc lattice. The cemented carbide with 10 wt.% of the $Co_{27.4}Cr_{13.8}Fe_{27.4}Ni_{27.4}Mo_4$ HEA with an fcc lattice had a hardness of 2141 HV and fracture toughness of 10.5 MPa.m$^{1/2}$. These values are higher than those for the typical WC–10 wt.% Co composite. The substitution of Co with HEAs also influences the phase transitions in the binder (between the fcc, bcc and hcp phases). These phase transformations can be successfully used for the purposeful modifications of the properties of the WC-HEA cemented carbides. The shape of the WC/binder interfaces (e.g., their faceting–roughening) can influence the mechanical properties of cemented carbides. The most possible reason for such a behavior is the modification of conditions for dislocation glide as well as the development and growth of cracks at the last stages of deformation. Thus, the substitution of a cobalt binder with HEAs is very promising for the further development of cemented carbides.

Keywords: cemented carbides; binder; high-entropy alloys; grain boundary wetting; phase transitions; phase diagrams

Citation: Straumal, B.; Konyashin, I. WC-Based Cemented Carbides with High Entropy Alloyed Binders: A Review. *Metals* **2023**, *13*, 171. https://doi.org/10.3390/met13010171

Academic Editor: Francisco Gil Coury

Received: 24 December 2022
Revised: 10 January 2023
Accepted: 11 January 2023
Published: 14 January 2023

1. Introduction

Cemented carbides, also known as hardmetals, have become one of the most important engineering materials since their invention in the early 1920s. WC-Co cemented carbides are used for numerous applications due to their unique combination of hardness, fracture toughness and abrasion resistance. In their simplest form, these materials consist of WC grains embedded in a ductile metallic binder, typically cobalt. The tungsten carbide–cobalt materials possess high hardness (up to nearly 20 GPa [1]), density (≈15 g/cm^3 [1,2] at 10 wt.% Co), fracture toughness (>10 MPa.m$^{1/2}$ at 10 wt.% Co depending on a WC mean grain size [3]) and strength (transverse rupture strength (TRS) of above 3000 MPa at 10 wt.% Co [1]). This unique combination of different properties makes cemented carbides the best-known materials for many applications. Unfortunately, the use of cobalt (T_{melt} = 1495 °C [2]) as a binder in cemented carbides is disadvantageous at high temperature, in strong corrosive media and in other harsh environments because of its poor corrosion resistance and high temperature resistance [4]. Additionally, the cobalt binder in WC-based cemented carbides has some health concerns because of its possible carcinogenic

effects [5]. Due to these health concerns as well as to tailor or improve the mechanical properties of WC-based cemented carbides, numerous attempts have been made to find alternative binders [6,7]. These attempts are listed in Table 1.

Table 1. Alternative binders for WC-based cemented carbides.

Group of Alternative Binders	Composition and Reference
Iron and iron-based alloys	Fe–Ni, Fe–Ni–Co, Fe–Cr, Fe–Al [8], Fe–Ni–C [9] 10 wt.% Fe [10] Fe–Ni, Fe–Ni–Co, Fe–Mn [11,12] Fe–Ni–Co [13,14] Fe–Cr–Ti(C,N) [15] Fe–Al–B [16] FeAl, Ni_3Al [17] Fe–Ni–Cr [18,19] Fe–Ni–Co [20] Alloyed κ-$W_9Fe_3C_4$, κ-$W_9Ni_3C_4$, and κ-W_9 $(Fe/Ni)_3C_4$ phases [21] Fe–Cu [22] Fe, FeAl [23–25] FeAl with VC and/or Cr_3C_2 [26] Fe_3Al [27] Fe–Mn [28,29] Fe–Ni–C [30] H13 Hudson tool steel [31] AISI 304 stainless steel [32–35] High vanadium tool steels PM 10 V and PM 15 V [36]
Cobalt-based alloys	Fe–Ni–Co [13,20] Fe–Cr–Co [37] Fe–Cu–Co [38] Fe–Cu–Ni–Co [39]
Carbide binders	Fe–Cr–Ti(C,N) [15] κ-$W_9Fe_3C_4$, κ-$W_9Ni_3C_4$, and κ-W_9 $(Fe/Ni)_3C_4$ phases [21] FeAl with VC and/or Cr_3C_2 [26], VC and Al [40], W_6Co_6C [41], ZrC [42], WCrC [43,44]
η-phases	W_2C, W_3Co_3C, W_4Co_2C, and W_6Co_6C [41], ZrC [42], WCrC [43,44], AgNi [45]
Various pure metals	Al [40], Cr [37], Cu [38,46], Al [47,48]
Nickel and nickel-based alloys	[7,10,12,17,18,39]

Some of these attempts to replace cobalt were quite successful, but not always. In many cases, they failed due to various reasons, such as the poor mechanical properties (e.g., fracture toughness, hardness, and transverse rupture strength—TRS) [12,13,17,22,25,26,35,36,38,42], the growth of large or abnormally large WC grains [7,29,30,40], the formation of deleterious phases [7,10,19,28–31,34,37] as well as poor densification behavior during sintering [26,33].

One can see that these attempts were made with pure metals [1,7,8,10,23,37,38,46–48], binary alloys [8,10,17,18,22,24,25,27–29,42,45], ternary [8–10,13,15–20,26,30,37–41,43,44] or ever quaternary alloys [21,26,30–36,39]. A very interesting attempt was to use the strengthening nanozones in the Co matrix, based on the Co_3W phase, with the Cu_3Au lattice [49].

The logical continuation of this way was to move up to even more complicated alloys. As a result, a new approach was recently elaborated, namely the substitution of cobalt binder with multicomponent alloys without any principal component. These alloys contain at least five components. Such alloys are also known as high-entropy alloys or HEAs [50]. HEAs usually have a densely packed crystal lattice (fcc, hcp or bcc) and contain only one multicomponent solid solution comprising at least five different elements. HEAs

possess elevated high-temperature hardness, wear-resistance and corrosion resistance. Disordered arrangements of atoms in the crystal lattice of HEAs prevent the diffusion mass transfer due to a strong lattice distortion effect. HEAs can allow the decreasing of the sintering temperature of cemented carbides and suppress the growth of WC grains during sintering [51]. They also ensure good WC wettability with the liquid binder. As a result, cemented carbides with HEA binders show excellent high-temperature hardness, high wear-resistance and improved fracture toughness [51]. The substitution of a cobalt binder with HEAs also influences the phase transitions in the binder (between the fcc, bcc and hcp phases) and affects the WC/binder interfaces (faceting–roughening). One can find further details on the WC-based cemented carbides with HEA binders in Refs. [50–70]; they are also discussed below in this review.

It should be mentioned that some conventional cemented carbide grades with a Co-based binder, containing either grain growth inhibitors (vanadium and chromium carbides) or cubic (Ti,Ta,Nb,W) C carbides (carbide grades for steel machining), can be considered as cemented carbides with HEA binders. In the first case, the binder comprises Co, V and Cr as well as W and C, which are usually dissolved in the binder, so that the formal requirement that the binder must be a solid solution of five chemical elements is formally satisfied. In the second case, the binder consists of six chemical elements: Co, Ti, Ta, Nb, W and C.

2. Refinement of WC Grains by Use of HEA Binders

The application of HEA binders can be used as an effective instrument for the refinement of WC grains. For example, Zhou et al. studied WC cemented carbides with equimolar AlFeCoNiCrTi HEA as a binder [51]. The AlFeCoNiCrTi HEA powders were prepared using high-energy ball milling. The WC-based cemented carbides were fabricated by use of a conventional powder metallurgy route. The WC–10 wt.% Co, WC–10 wt.% HEA and WC–20 wt.% HEA powders were milled with tungsten carbide balls in a planetary ball-mill. The dried mixed powders were sintered at a pressure of 10 MPa at 1500 °C for 2 h. The AlFeCoNiCrTi HEA had a bcc lattice. The size of the WC grains in the WC–10 wt.% Co alloys was about 1 μm, whereas in the WC–10 wt.% HEA and WC–20 wt.% HEA alloys, the WC mean grain size was at least five times smaller. Thus, the substitution of cobalt binder with the bcc HEA drastically changed the WC grain size.

Another example of WC grain refinement with HEA binders was give in the work of Chen et al. [54]. In their work, $Co_xFeNiCrCu$ (x = 1, 1.5, 2, 2.5) HEAs were mechanically alloyed using high-energy ball milling from high purity (99.99 wt%) metals at a rotation rate of 400 rpm for 48 h, and with a ball-to-powder weight ratio of 6:1. The WC-HEA powders were poured into a ∅20 graphite die and sintered in a spark plasma sintering (SPS) system at a uniaxial pressure of 30 MPa for 8 min at 1300, 1350, 1400 and 1450 °C. The conventional WC–10 wt.% Co alloys were also prepared for comparison. In Figure 1, the average size of the WC grains in the conventional WC–10 wt.% Co alloy and in WC-HEA ($Co_xFeNiCrCu$, x = 1, 1.5, 2, 2.5) alloys sintered at 1400 °C is shown [54]. The CoFeNiCrCu HEA contained a mixture of fcc and bcc phases. The substitution of the cobalt binder with the CoFeNiCrCu HEA lead to a grain size decrease from 630 nm to 400 nm. The WC grain size slightly increased with an increasing cobalt content in the HEA. Thus, the usage of the CoFeNiCrCu HEA binder with a mixture of fcc and bcc phases was less effective for WC grain refinement in comparison with AlFeCoNiCrTi HEA having one bcc phase [51].

A third important example of HEA with an fcc lattice was given in the work of Velo et al. [57]. An equimolar CoCrFeNiMn HEA with an fcc crystal structure was prepared using ball milling of the powder mixture. The WC powder was taken in its as-delivered state or ball milled for 2 or 4 h. These three kinds of WC powder were mixed with 10, 20 or 30 vol.% of the milled HEA powder and sintered at 1450 °C for 60 min. A minimal WC grain size of 300 nm was obtained for the sample of WC milled for 2 h with 10 mol.% of HEA. A maximal WC grain size of 760 nm was obtained for the sample with WC milled for 2 h and 30 mol.% of HEA. Thus, the obtained WC grain size with an fcc binder was higher than in the composites with bcc [51] and bcc + fcc binders [54]. It should be also noted that

the HEAs mentioned above [51,54] contained chromium, which is known to be a strong grain growth inhibitor, so the refinement of WC grains is expected.

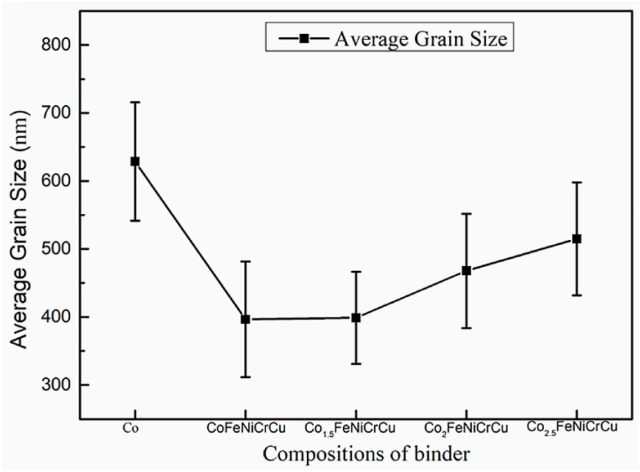

Figure 1. The average size of WC grains in the WC–10 wt.% Co alloy and in the WC-HEA ($Co_xFeNiCrCu$, x = 1, 1.5, 2, 2.5) alloys sintered at 1400 °C. Reprinted with permission from Ref. [54]. Copyright 2022 Elsevier.

3. Corrosion Resistance and Oxidation Behavior

Zhou et al. studied the corrosion resistance of WC–10 wt.% Co, WC–10 wt.% HEA and WC–20 wt.% HEA alloys [51]. The studied AlFeCoNiCrTi HEA had a bcc lattice. The corrosion resistance of these alloys was tested electrochemically in a 0.1 M sulphuric acid solution. Table 2 contains the electrochemical characteristic parameters and polarization curves, respectively. The passive and over-passive regions are clearly seen in all three alloys. The passive region in the WC–10 wt.% Co alloy is wider in comparison with the two other alloys. This means a higher corrosion potential of the WC–10 wt.% Co alloy. The WC–10 wt.% HEA and WC–20 wt.% HEA have a small platform in the anode polarization region (before the passive region). Differently, in the WC–10 wt.% Co alloy, a similar small platform occurs inside the passive region, which means that the HEA binder is more passive than the cobalt one.

Table 2. Electrochemical corrosion parameters of WC-based cemented carbides with Co and HEA binders [51].

Alloys, Reference	E_{corr}, V	I_{corr}, mA cm^{-2}	Solution
WC–10 wt.%Co [51]	–0.272	14.371	0.1 M sulphuric acid
WC–10 wt.% HEA [51]	–0.281	3.404	0.1 M sulphuric acid
WC–20 wt.% HEA [51]	–0.289	1.549	0.1 M sulphuric acid

One can see in Table 2 that the WC–10 wt.% Co alloy has a higher E_{corr} in comparison with the WC–10 wt.% HEA and WC–20 wt.% HEA alloys, which means that the corrosion resistance of WC–10 wt.% Co is the lowest among the three alloys. The E_{corr} of WC–10 wt.% HEA and WC–20 wt.% HEA is almost the same. This means that the corrosion resistance of these cemented carbides depends mainly on the type of the binder, but not on the binder content. The corrosion current density I_{corr} for WC–10 wt.% Co is larger than I_{corr} for WC–10 wt.% HEA and WC–20 wt.% HEA; in other words, the WC–HEA alloys possess higher corrosion resistance than the WC–Co alloy. The I_{corr} of WC–10 wt.% HEA is two times higher than that of WC–20 wt.% HEA, which means that the binder content and the corrosion rate are inversely proportional.

Luo et al. examined the isothermal oxidation behavior of the conventional WC-Co cemented carbides and cemented carbides with HEA binders with the composition

$Al_xCoCrCuFeNi$ (x = 0, 0.5, 1.0, 1.5) [63]. Such alloys contain a single fcc phase for $x < 0.8$ and a mixture of bcc and fcc phases at $x > 0.8$.

The experiments were conducted at 600–800 °C in air using the thermogravimetric method. The oxidation rate of the WC-HEA decreased with an increasing aluminum concentration in the HEA binder. In particular, the specific mass gains of the composites with HEA binder were at least 20% smaller than that of the conventional WC–Co cemented carbide. A further decrease in specific mass gain from 61.89 to 24.55 mg/cm^2 occurs when the HEA content increases from 5 to 20 wt. %. It should be also noted that with the increase in Al content, a transition takes place from a single phase fcc structure of HEA to a bcc + fcc two-phase one. Figure 2 shows the scheme for the steps of the oxidation process for the WC-HEA alloy. It starts from the selective oxidation of the HEA binder phase (Figure 2a), followed by the simultaneous oxidation of the HEA and the WC phases (Figure 2b,c), and finishes with the growth of the oxide layer accompanied by swelling (Figure 2d,e).

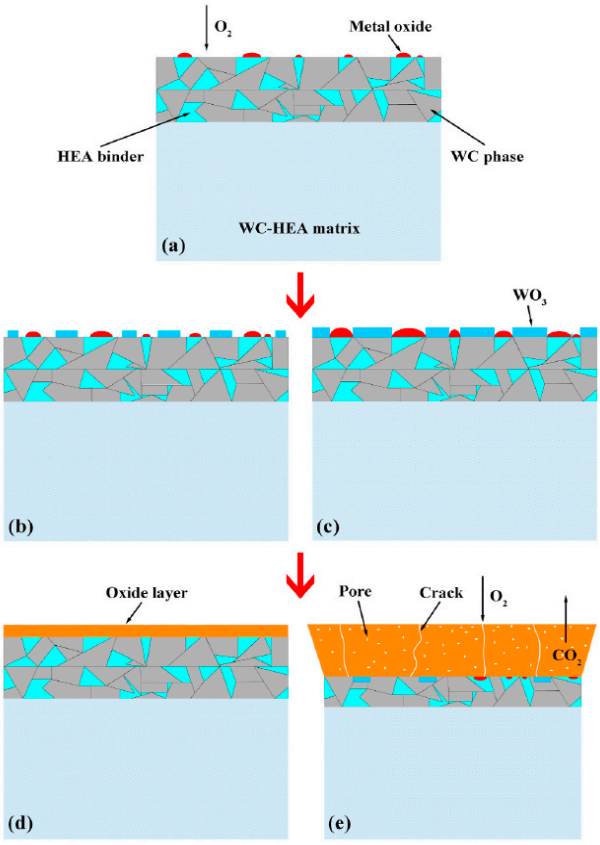

Figure 2. The schematic diagram of the oxidation process for the WC-HEA: (**a**) selective oxidation of the HEA binder phase; (**b**,**c**) simultaneous oxidation of the HEA and the WC phases; and (**d**,**e**) growth of the oxide layer accompanied by swelling. Reprinted with permission from Ref. [63]. Copyright 2021 Elsevier.

It should be noted that the HEAs mentioned above contained chromium and nickel, the oxidation and corrosion resistance of which are greater than those of cobalt, so the improved oxidation and corrosion resistance of the cemented carbides with HEA binders can be expected. In addition, further investigations with HEAs containing various elements are very promising to improve oxidation and corrosion resistance.

4. Hardness and Fracture Toughness

In Ref. [51], the WC–10 wt.% Co, WC–10 wt.% HEA and WC–20 wt.% HEA alloys were prepared using high-energy ball milling with an equimolar AlFeCoNiCrTi HEA. The mixed HEA and WC powders were sintered at 10 MPa and 1500 °C for 2 h. The studied AlFeCoNiCrTi HEA had a bcc lattice. The Vickers hardness, fracture toughness and

compression strength of cemented carbides with the HEA binder increased in comparison with the conventional WC–10 wt.% Co alloy (see Table 3).

Table 3. Vickers hardness, fracture toughness, compression strength, transverse rupture strength and ultimate tensile strength of WC-based cemented carbides with Co and HEA binders.

Alloys, Compositions and Sintering Temperatures °C	Hardness, Vickers Units	Fracture Toughness, MPa.m$^{1/2}$	Compression Strength, MPa
WC–10 wt.%Co, 1500 °C [51]	1910	8.10	3595
WC–10 wt.% HEA, 1500 °C [51]	2231	8.33	5219
WC–20 wt.% HEA, 1500 °C [51]	2358	12.10	5420
WC–10 wt.% HEA, 1300 °C [52]	1200	7.5	2110
WC–10 wt.% HEA, 1400 °C [52]	2160	7.0	4395
WC–10 wt.% HEA, 1450 °C [52]	2090	6.9	4125
WC–20 wt.% HEA, 1300 °C [52]	1600	9.2	3530
WC–20 wt.% HEA, 1400 °C [52]	1701	9.5	3644
WC–20 wt.% HEA, 1450 °C [52]	1640	9.9	3507
WC–10 wt.%Co, 1500 °C [71]	1784	7.5	-
WC-10CoFeNiCrCu, 1300 °C [54]	1570	9.2	-
WC-10CoFeNiCrCu, 1350 °C [54]	1810	11.2	-
WC-10CoFeNiCrCu, 1400 °C [54]	1952	10.8	-
WC-10CoFeNiCrCu, 1450 °C [54]	1870	10.7	-
Conventional WC-10 wt.%Co [54]	1544	9.1	-
WC-10 Al_xCoCrCuFeNi, x = 0 [52]	1820	9.8	-
WC-10 Al_xCoCrCuFeNi, x = 0.5 [52]	2070	10.3	-
WC-10 Al_xCoCrCuFeNi, x = 1.0 [52]	2040	9.9	-
WC-10 Al_xCoCrCuFeNi, x = 1.5 [52]	2130	9.8	-
WC–10 wt.%Co [56]	1458	10.1	-
WC–7.5 wt.%Co–2.5 wt.% HEA [56]	1550	8.2	-
WC–5 wt.%Co–5 wt.% HEA [56]	1679	6.4	-
WC–10 wt.% HEA [56]	1004	5.4	-
WC–10 wt.%Co–5 wt.% HEA [56]	1421	10.8	-
WC–10 wt.%Co–10 wt.% HEA [56]	1222	17.8	-
WC–10 wt.%FeNiZr, 2000 A [59]	1581	-	-
WC–10 wt.%FeNiZr, 1850 A [59]	1550	-	-
WC–10 wt.%FeNiZr, 1800 A [59]	1540	-	-
WC–Co [70]	-	12.1–16.2	-
WC–CoNiFe [70]	-	13.2–17.8	-
WC–10Co7Ni2Fe1Cr4.5C (wt.%) [62]	1080	-	Transverse rupture strength 1800
WC–10Co7Ni2Fe1Cr4.7C (wt.%) [62]	1000	-	1700
WC–10Co7Ni2Fe1Cr4.9C (wt.%) [62]	950	-	3450
WC–CoCrFeNi [65]	1394	-	Ultimate tensile strength 629
WC– $(CoCrFeNi)_{0.96}W_{0.04}$ [65]	1712	-	687
WC–10 wt.%($Co_{27.4}Cr_{13.8}Fe_{27.4}Ni_{27.4}Mo_4$) [67]	2141	10.5	-
WC–20 wt.% ($Co_{27.4}Cr_{13.8}Fe_{27.4}Ni_{27.4}Mo_4$) [67]	2039	9.5	-

Zhou et al. prepared WC-based cemented carbides with a binder of an equimolar AlCrFeCoNi HEA [52]. The high-purity (99.99 wt.%) Al, Fe, Co, Cr and Ni metals were first melted in a vacuum in an induction furnace. The HEA melt was then atomized in a high-purity argon atmosphere. The atomized powders were sieved through a 200-mesh screen. The mean grain size of the WC powders employed was 200 nm. The powders of WC–10 wt.% HEA and WC–20 wt.% HEA were prepared in a planetary ball mill. The green samples were first heated in a vacuum up to 500 °C at a heating rate of 10 °C/min, and then heated up to 1200 °C at a heating rate of 20 °C/min, followed by heating up to the final sintering temperatures of 1400 °C and 1450 °C at a heating rate of 20 °C/min. The precipitation of Al from the AlCrFeCoNi alloy causes the bcc-to-fcc transformation of the high entropy alloy.

The fracture toughness and hardness of these WC-HEA composites [52] are given in Table 3. Their values firstly increase and then decrease with the increasing sintering temperature. The liquid phase sintering was not fully completed at a temperature of 1300 °C. Therefore, the WC grains grew mainly by aggregation and recrystallization. The hardness of the samples was reduced due to the abnormal WC grain growth and high porosity of the samples sintered at 1300 °C. An increase in the sintering temperature up to 1400 °C made the dissolution and re-precipitation of WC grains easier. On the other hand, it enhanced WC grain coarsening, which can result in poor mechanical properties. When the sintering temperature increased up to 1450 °C, the hardness decreased further. Therefore, the samples sintered at 1400 °C (both WC–10 wt.% HEA and WC–20 wt.% HEA) possessed the highest Vickers hardness. The binder content significantly affects the fracture toughness. Thus, the fracture toughness of the WC–10 wt.% HEA samples decreased with the increasing sintering temperature. On the contrary, the hardness value of the WC–20 wt.% HEA alloy increased with the increasing sintering temperature. In the WC–10 wt.% HEA samples, the fracture toughness was inversely proportional to hardness. When the HEA content increased up to 20 wt.%, the fracture toughness of the samples became higher.

In the work of Chen et al. [54] the WC–10 wt.% Co and WC-Co_xFeNiCrCu (x = 1, 1.5, 2, 2.5) HEA alloys were sintered from pure powders under uniaxial pressure of 30 MPa at 1300, 1350, 1400 and 1450 °C. The studied HEA had an fcc lattice. The fracture toughness and hardness of the WC-10CoFeNiCrCu composites [54] are given in Table 3. An increase in the sintering temperature eliminated the porosity and increased density, thus improving the hardness values. The relative density after sintering at 1400 °C and 1450 °C was almost equal, but sintering at a higher temperature lead to a larger WC mean grain size. The fracture toughness increased with the elimination of pores. In addition, coarsening WC grains resulted in an increased number of WC/WC grain boundaries (GBs). This circumstance increased also the probability of crack propagation along the WC/WC GBs. WC has a significantly lower fracture toughness in comparison with the HEA binder, so that the overall fracture toughness of the alloy decreased. This work indicates that the HEA has the potential to replace the conventional Co as a new binder, because of its finer grain and high hardness.

Luo et al. used the elemental powders of Al, Co, Cr, Cu, Fe, and Ni of >99.5 wt.% purity and an average particle size below 45 μm to produce Al_xCoCrCuFeNi HEAs [53]. The starting WC powders had a purity of >99% and a mean grain size of about 0.9 μm. Ball-milled Al_xCoCrCuFeNi (with x = 0, 0.5, 1.0, 1.5) HEA powders were used as binders to produce WC-10 wt.% HEA cemented carbides using SPS. Such alloys contain a single fcc phase for $x < 0.8$ and a mixture of bcc and fcc phases at $x > 0.8$. The relative density of the WC-HEA alloys increased from 97 to 98.9% with an increasing aluminum content, as well as Vickers hardness. The fracture toughness first increased with the increasing aluminum content to a value of 10.3 MPa $m^{1/2}$ at x = 0.5, and afterwards decreased. Thus, an ultrafine WC-HEA alloy with the best mechanical properties can be produced with the $Al_{0.5}$CoCrCuFeNi HEA as a binder. One should mention that a relative density of about 99% obtained using SPS is insufficient for the majority of applications; the present state of

the art in the carbide industry corresponds to a density of 100.0% obtained as a result of sintering in a vacuum followed by HIPing in Ar at high pressures.

In Ref. [56], WC-Co/CrMnFeCoNi composites were manufactured by Dong et al. using sintering at 1410 °C. CrMnFeCoNi HEA is known as Cantor alloy and possesses a single-phase fcc structure. The binder contained different amounts of cobalt and is an equimolar HEA, so that the following cemented carbides were produced: WC–10 wt.% Co, WC–7.5 wt.% Co–2.5 wt.% HEA, WC–5 wt.% Co–5 wt.% HEA, WC–10 wt.% HEA, WC–10 wt.% Co–5 wt.% HEA and WC–10 wt.% Co–10 wt.% HEA. The Vickers hardness as well as fracture toughness increased with the increasing HEA content (see Table 3).

Li et al. fabricated WC–CoCrFeNi and WC–$(CoCrFeNi)_{0.96}W_{0.04}$ cemented carbides with HEA binders using arc melting in a water-cooled copper hearth under an Ar atmosphere, using high purity Co, Cr, Fe, Ni, and W powders (>99.9%) [65]. All samples were homogenized at 1200 °C for 5 h and subsequently forged at 1200 °C, which lead to a 50% reduction in their thickness. The HEA binder contained hcp and fcc phases. Then, the forged samples were heat-treated at 1200 °C for 6 min with water quenching, followed by room temperature rolling to a 40% reduction in thickness. Finally, the samples were heat treated at 1000 °C again for 6 min to obtain fully recrystallized structures. The hardness of the studied samples increased with increasing tungsten content.

In Ref. [65], cemented carbides with fcc HEA binders WC–10 wt. % ($Co_{27.4}Cr_{13.8}Fe_{27.4}Ni_{27.4}Mo_4$) and WC–10 wt. % ($Co_{27.4}Cr_{13.8}Fe_{27.4}Ni_{27.4}Mo_4$) were sintered at 1200 °C for 15 min and a pressure of 50 MPa using the SPS technique. The HEA binder was designed using Thermo-Calc calculations. Compared to a commercial WC–Co material, WC–10 wt.% HEA composites exhibit higher hardness and fracture toughness (21 GPa and 10.5 MPa $m^{1/2}$, respectively).

Pittari et al. sintered a WC powder with 10 wt.% of an equimolar FeNiZr medium-entropy alloy (MEA) using the field-assisted sintering technique with heating at a current increase rate of 100, 150 and 200 A/s up to a current value of 1800, 1850 or 2000 A [59]. The resulting hardness of this composite lay between 1540 and 1582 Vickers units (see Table 3). In Ref. [70], the WC-CoNiFe and WC-Co cemented carbides with different grain sizes were prepared using sintering including hot isostatic pressing (Sinter-HIP). Their fracture behavior was evaluated. The results showed that WC-CoNiFe had a slightly higher fracture toughness than that of WC-Co (see Table 3). Thus, the application of medium-entropy alloys binders (MEAs) instead of pure cobalt does not improve the mechanical properties of cemented carbides as strongly as the usage of HEAs.

Thus, the best values of hardness (2358 HV), fracture toughness (12.1 MPa.$m^{1/2}$) and compression strength (5420 MPa) were obtained for the WC with 20 wt.% of equimolar bcc AlFeCoNiCrTi HEA sintered at 1500 °C [51]. The second best values of hardness (2141 HV) and fracture toughness (10.5 MPa.$m^{1/2}$) were obtained for the WC with 10 wt.% fcc $Co_{27.4}Cr_{13.8}Fe_{27.4}Ni_{27.4}Mo_4$ HEA [67]. These values are higher than those for the typical WC–10 wt.%Co composite [51].

What is the difference in the toughening mechanisms in the WC-HEA cemented carbides in comparison with those with a cobalt binder? These are generally speaking crack deflection, WC grain pull-out and crack bridging. The high deformability of HEA binders surrounding the hard WC crystallites is due to extensive plastic stretching in the crack. When the crack spreads in the HEA binder, the binder phase necks to a point or to a line [53]. This indicates crack bridging. As a result, the crack opening is inhibited behind the crack tip contributing to the improvement of toughness. The fracture toughness of the WC cemented carbides with HEA binders can also be improved by the crack deflections resulting from an intergranular fracture. The crack deflections and the total length of fracture paths can be increased thanks to the grain refinement and higher volume fraction of abnormal WC grains. It means that a higher amount of energy can be consumed during the propagation of a crack [53].

In addition, the pulling out of WC grains can additionally consume energy during crack propagation. The observations of cracks demonstrate that numerous elongated WC grains at the interfaces between WC crystallites and the HEA binder are pulled out [53].

The resulting holes in the HEA binder are highly visible on the fracture surfaces. Thus, the pulling out of WC grains also consumes energy. As a result, the inhibition of crack extension improves the fracture toughness of WC-HEA cemented carbides.

5. Phase Transitions in the Binder

The phase transitions in the binder are critical for its homogeneity. If the binder consists of a multi-component alloy without a major component, it is possible that various phases will precipitate during the cooling or during the sintering. The alloy will freeze into a single-phase one if the diffusion is slowed down. This is the case when the entropy contribution to the Gibbs energy dominates. If the diffusion stops at a temperature where the entropy term is small, the system may be a multiphase mixture instead of single-phase one.

In the WC-based cemented carbides with an equimolar AlCrFeCoNi HEA binder [52], the precipitation of Al during sintering results in a transformation from the body-centered cubic (bcc) to face-centered cubic (fcc) structure of the HEA binder. The precipitated Al reacted with oxygen forming an alumina film around the remaining pores. The final HEA/WC composite material consists of two or three hard phases (WC and η-phases M_3W_3C and $M_3W_9C_4$) as well as a remaining HEA binder with an fcc crystal structure [52].

Luo et al. [53] produced WC-HEA cemented carbides with a HEA binder of $Al_xCoCrCuFeNi$ (x = 0, 0.5, 1.0, 1.5) HEA using SPS. The major phases of the HEA binders with different Al contents transformed after sintering into phases with an fcc crystal structure. Thus, the fcc phase is likely a phase stable at high temperature for $Al_xCoCrCuFeNi$ HEAs. No η-phase or deteriorating metal oxide properties of cemented carbides were detected in the XRD patterns during the preparation of the WC-HEA samples, which is beneficial for the mechanical properties of WC-$Al_xCoCrCuFeNi$ composites [53].

According to the results of Ref. [56], the HEA binder in the cemented carbide WC-Co/CrMnFeCoNi does not only comprise a single phase with an fcc crystal lattice. After addition of HEAs to WC-Co composites, an η-carbide phase inevitably forms due to the reaction between WC and the HEA components during liquid phase sintering. When the HEA completely replaces cobalt as the binder, the sample contains a lot of cobalt pools and pores, which significantly deteriorate the mechanical properties.

In the work of Holmström et al., the HEA binder phase consisted of a CoCrFeNi alloy containing dissolved tungsten and carbon [58]. Holmström et al. combined the thermodynamic and first principle calculations and established the HEA composition corresponding to a martensitic transformation of the hcp phase to the fcc one; the HEA is characterized by certain carbon and tungsten solubilities. The resulting cemented carbide with a HEA binder phase withstood much higher cutting speeds in metal-cutting than conventional WC-Co cemented carbides [58]. The increased durability of cutting tools was also observed for cemented carbides with CoFeCu and CoMoTi medium entropy alloy binders [60].

Thus, the phase transformations in the WC-HEA cemented carbides can be successfully used for the purposeful modifications of their properties. Especially promising can be the way from single-phase HEAs towards two- or multiple-phase ones. Well-tuned thermal treatments could allow the further improvement of HEA binders; for example with strengthening nanoprecipitates, as was conducted earlier with a conventional Co binder [49].

6. Faceting–Roughening of WC/Binder Interfaces

Usually, WC grains in sintered cemented carbides with a cobalt binder have a shape of truncated trigonal prisms and are perfectly faceted (see for example Figure 3 [72,73]). However, it is well known that faceted (flat) surfaces or interfaces can become curved as a result of the so-called faceting–roughening phase transformation [74,75]. The transition from the faceted to the rough (curved) shape can take place with a change in the misorientation or inclination of interfaces [76,77], temperature increase [78,79] or change in the composition [80]. In Ref. [61], the conventional cobalt binder was substituted in cemented carbides with an equimolar CoCr-

CuFeNi HEA and two different HEAs with aluminum additions, namely $Al_{0.5}$CoCrCuFeNi and Al_2CoCrCuFeNi. The microstructure of such cemented carbides, sintered at 1500 °C in a vacuum for 2 h, is shown in Figure 4, redrawn from Ref. [61].

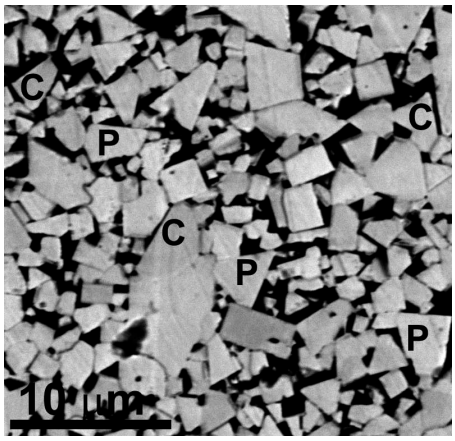

Figure 3. SEM micrograph of the ultra-coarse cemented carbide after liquid-phase sintering at 1380 °C. WC grains appear bright, and Co/binder appears dark. Letters indicate C: WC/WC grain boundaries completely wetted by the Co-based melt with zero contact angle; and P: WC/WC grain boundaries partially (incompletely) wetted by the melt with a non-zero contact angle. Reprinted with permission from Ref. [72]. Copyright 2017 Elsevier.

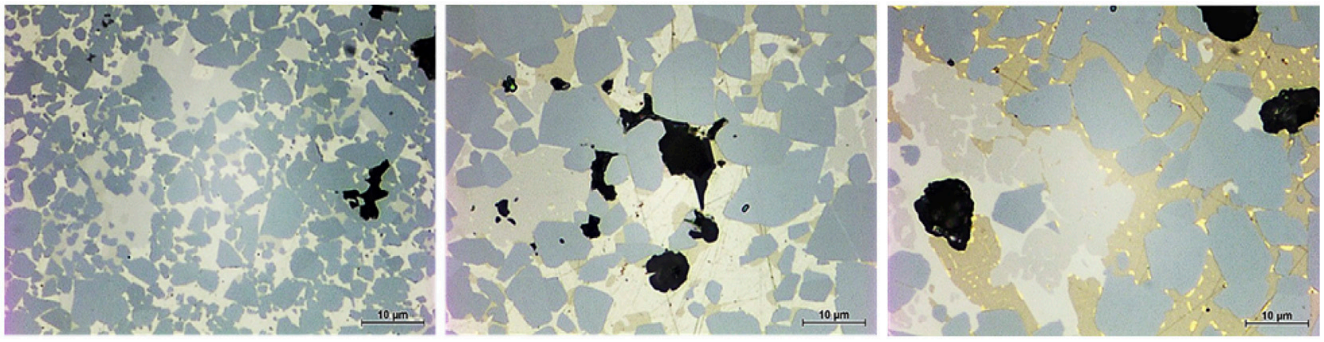

CoCrCuFeNi $Al_{0.5}$CoCrCuFeNi Al_2CoCrCuFeNi

Figure 4. Microstructures of cemented carbides with the CoCrCuFeNi, $Al_{0.5}$CoCrCuFeNi and Al_2CoCrCuFeNi HEA binders sintered at 1500 °C in a vacuum for 2 h. Reprinted with permission from Ref. [61]. Copyright 2019 Elsevier.

It can be clearly seen that the shape of WC grains (they appear grey in Figure 4) strongly differs from that in conventional cemented carbides. The WC grains of cemented carbides obtained according to Ref. [61] are rounded and possess many fewer flat facets than those reported in Refs. [73,81]. It appears that the WC grains in the composite with the $Al_{0.5}$CoCrCuFeNi HEA binders are a little bit more faceted than in the CoCrCuFeNi and Al_2CoCrCuFeNi HEA binders (see Figure 4, redrawn from Ref. [61]). In other words, the substitution of the conventional cobalt binder with HEA binders can lead to the faceting–roughening transition of the WC/binder interfaces. Such shape change in the WC/binder interfaces can, in turn, affect the phenomena of crack initiation and propagation in cemented carbides subjected to high impact loads and, thus, improve or deteriorate their mechanical properties.

The results of Qian et al. give a good example of how the shape of WC grains can affect the mechanical properties of cemented carbides [70]. WC-CoNiFe and WC-Co cemented carbides with different grain sizes were prepared using vacuum sintering followed by hot isostatic pressing (Sinter-HIP) [70]. The WC-CoNiFe material had a higher fracture toughness than WC-Co (see Table 3). The fracture toughness and fatigue crack growth (FCG) were closely related to the parameters of the cemented carbides' microstructure. The

fracture toughness increased via ductile ligament bridging and crack deflection, as the mean free path of the binder phase (λ_{Co}) increased, or the contiguity of the carbide phase (CWC) decreased. The fatigue fracture mode showed a transition from a cleavage-like brittle fracture to a ductile dimple-like fracture. The fatigue sensitivity of cemented carbides was directly related to the fracture toughness [70].

Qian et al. prepared cemented carbide WC-10Co-7Ni-2Fe-1Cr (wt.%) with different carbon contents (4.5, 4.7 and 4.9 wt.%) using vacuum sintering followed by hot isostatic pressing (Sinter-HIP) [62]. The alloys contained clusters consisting of WC grains fully surrounded by an η-phase (Figure 5a). These WC grains were rounded and had fewer flat facets than those surrounded by the 10Co-7Ni-2Fe-1Cr binder (Figure 5b). The η-phase aggregates in large clusters with the increasing carbon content, which leads to a decrease in hardness and an increase in TRS (see Table 3). The shape change in the WC grains could be at least partially responsible for this effect.

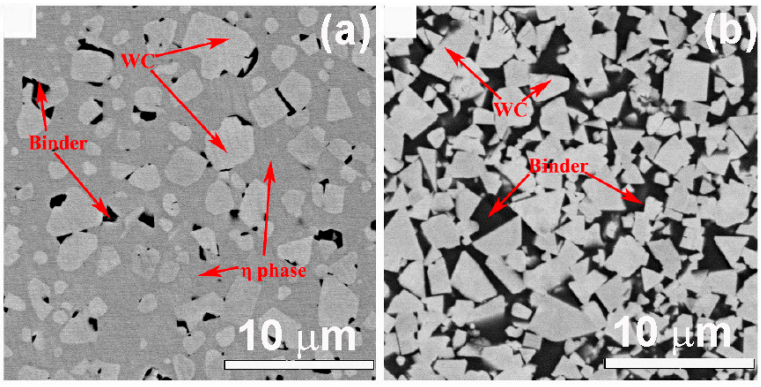

Figure 5. Cemented carbide microstructures indicating WC grains surrounded by the η-phase (**a**) and CoNiFeCrC-based binder (**b**). Reprinted with permission from Ref. [62]. Copyright 2022 Elsevier.

How we can understand the influence of the faceting/roughening of WC grains on the mechanical properties of WC-based cemented carbides? Crack deflection and bridging are the main toughening mechanism for WC grains. In case of strong crack deflection on WC grains, it is determined by the characteristics of the WC crystallites. The WC crystal possesses a close-packed hexagonal crystal structure. It has only one slip family {1010} ⟨1123⟩ in the unit cell and four independent slip systems [70].

As a result, the transgranular propagation is more complicated compared with intergranular propagation. If a propagating crack meets a WC grain, it is not very probable that the slip surface and direction are the same as the original. As a result, crack deflection or branching takes place when the crack starts to propagate through WC grains. In case of less faceted WC grains, the intergranular crack propagation along curved interfaces is also more complicated in comparison with flat and faceted WC grains. Thus, the crack paths are more tortuous when they follow larger and more rounded WC grains. The cracks exhibit more pronounced and frequent deflections or branches. Such cemented carbides exhibit higher toughness. In other words, the fracture changes from a cleavage-like brittle one to a ductile dimple fracture.

Thus, the shape change in the WC grains (e.g., faceting–roughening of WC/binder interface) can influence the mechanical properties of cemented carbides. The most possible reason for such a behavior is the modification of conditions for dislocation glide as well as for the development and growth of cracks at the last stages of deformation. The control of the shape of WC crystallites, by changing the composition of the HEA binder as well as the well-tuned thermal treatment, is very promising for the further development of cemented carbides.

7. Conclusions

The substitution of a cobalt binder with HEAs can lead to the refinement of WC grains. It can also lead to an increase in the hardness, fracture toughness, and corrosion- and

oxidation-resistance of cemented carbides. The best values of hardness (2358 HV), fracture toughness (12.1 MPa.m$^{1/2}$) and compression strength (5420 MPa) were obtained for the WC with 20 wt.% of equimolar bcc AlFeCoNiCrTi HEA sintered at 1500 °C [51]. The second best values of hardness (2141 HV) and fracture toughness (10.5 MPa.m$^{1/2}$) were obtained for the WC with 10 wt.% fcc $Co_{27.4}Cr_{13.8}Fe_{27.4}Ni_{27.4}Mo_4$ HEA [67]. The substitution of Co with HEA also influences the phase transformations in the binder (between the fcc, bcc and hcp phases). These phase transformations can be successfully used for the purposeful modifications of the properties of the WC-HEA cemented carbides. Especially promising can be the way from single-phase HEAs towards two- or multiple-phase ones. In particular, one can use the phenomenon of grain boundary (GB) wetting already observed in HEAs [82–84]. The application of GB wetting allows us to purposely arrange the second phase in HEAs along GBs in the form of continuous layers or regular chains of lenticular precipitates.

Last but not least, the shape change in the WC grains (e.g., the faceting–roughening of the WC/binder interface) can influence the mechanical properties of cemented carbides. The most possible reason for such a behavior is the modification of conditions for dislocation glide as well as for the development and growth of cracks at the last stages of deformation. The well-tuned thermal treatments of HEA binders could allow the further improvement of the HEA binders; for example, with shape change in WC crystallites or the introduction of strengthening nanoprecipitates, as was conducted earlier with a conventional Co binder [49]. Therefore, the substitution of a cobalt binder with HEAs is very promising for the further development of cemented carbides.

Author Contributions: Conceptualization, B.S. and I.K.; methodology, B.S.; formal analysis, I.K.; writing—original draft preparation, B.S.; writing—review and editing, I.K.; supervision, I.K.; project administration, B.S.; funding acquisition, B.S. All authors have read and agreed to the published version of the manuscript.

Funding: This research was funded by Russian Science Foundation, grant number 22-22-00511, https://rscf.ru/project/22-22-00511/ (accessed on 24 December 2022).

Institutional Review Board Statement: Not applicable.

Informed Consent Statement: Not applicable.

Data Availability Statement: Data are contained within the article.

Acknowledgments: The authors thank L.N. Shchur, E. Konstantinova and D. Kagramanian for fruitful discussions.

Conflicts of Interest: The authors declare no conflict of interest. The funders had no role in the design of the study; in the collection, analyses or interpretation of data; in the writing of the manuscript or in the decision to publish the results.

References

1. Cardarelli, F. *Materials Handbook: A Concise Desktop Reference*; Springer Science & Business Media: Berlin/Heidelberg, Germany, 2008.
2. Haynes, W.M. *CRC Handbook of Chemistry and Physics*; CRC Press: Boca Raton, FL, USA, 2014.
3. Swab, J.J.; Wright, J.C. Application of ASTM C1421 to WC-Co fracture toughness measurement. *Int. J. Refract. Met. Hard Mater.* **2016**, *58*, 8–13. [CrossRef]
4. Kwak, B.W.; Song, J.H.; Kim, B.S.; Shon, I.J. Mechanical properties and rapid sintering of nanostructured WC and WC-$TiAl_3$ hard materials by the pulsed current activated heating. *Int. J. Refract. Met. Hard Mater.* **2016**, *54*, 244–250. [CrossRef]
5. Huang, B.; Chen, L.D.; Bai, S.Q. Bulk ultrafine binderless WC prepared by spark plasma sintering. *Scripta Mater.* **2006**, *54*, 441–445. [CrossRef]
6. Norgren, S.; Holmstrom, E.; Linder, D. Cemented Carbide with Alternative. Binder. Patent US 11 213 892 B2, 4 January 2022.
7. Wittmann, B.; Schubert, W.D.; Lux, B. WC grain growth and grain growth inhibition in nickel and iron binder hardmetals. *Int. J. Refract. Met. Hard Mater.* **2002**, *20*, 51–60. [CrossRef]
8. Fernandes, C.M.; Senos, A.M.R. Cemented carbide phase diagrams: A review. *Int. J. Refract. Met. Hard Mater.* **2011**, *29*, 405–418. [CrossRef]
9. Gonzalez, R.; Echeberria, J.; Sanchez, J.M.; Castro, F. WC-(Fe,Ni,C) hardmetals with improved toughness through isothermal heat-treatments. *J. Mater. Sci.* **1995**, *30*, 3435–3439. [CrossRef]

10. Shon, I.J.; Jeong, I.K.; Ko, I.Y.; Doh, J.M.; Woo, K.D. Sintering behavior and mechanical properties of WC-10Co, WC-10Ni and WC-10Fe hard materials produced by high-frequency induction heated sintering. *Ceram. Int.* **2009**, *35*, 339–344. [CrossRef]
11. Schubert, W.D.; Fugger, M.; Wittmann, B.; Useldinger, R. Aspects of sintering of cemented carbides with Fe-based binders. *Int. J. Refract. Met. Hard Mater.* **2015**, *49*, 110–123. [CrossRef]
12. Norgren, S.; Garcia, J.; Blomqvist, A.; Yin, L. Trends in the P/M hard metal industry. *Int. J. Refract. Met. Hard Mater.* **2015**, *48*, 31–45. [CrossRef]
13. Gille, G.; Bredthauer, J.; Gries, B.; Mende, B.; Heinrich, W. Advanced and new grades of WC and binder powder-their properties and application. *Int. J. Refract. Met. Hard Mater.* **2000**, *18*, 87–102. [CrossRef]
14. Garcia, J. Investigations on kinetics of formation of fcc-free surface layers on cemented carbides with Fe-Ni-Co binders. *Int. J. Refract. Met. Hard Mater.* **2011**, *29*, 306–311. [CrossRef]
15. Alvaredo, P.; Tsipas, S.A.; Gordo, E. Influence of carbon content on the sinterability of an FeCr matrix cermet reinforced with TiCN. *Int. J. Refract. Met. Hard Mater.* **2013**, *36*, 283–288. [CrossRef]
16. Habibi Rad, M.; Ahmadian, M.; Golozar, M.A. Investigation of the corrosion behavior of WC–FeAl–B composites in aqueous media. *Int. J. Refract. Met. Hard Mater.* **2012**, *35*, 62–69. [CrossRef]
17. Ahmadian, M.; Wexler, D.; Calka, A.; Chandra, T. Liquid phase sintering of WC-FeAl and WC-Ni_3Al composites with and without boron. *Mater. Sci. Forum* **2003**, *426–432*, 1951–1956. [CrossRef]
18. Fernandes, C.M.; Senos, A.M.R.; Vieira, M.T.; Antunes, J.M. Mechanical characterization of composites prepared from WC powders coated with Ni rich binders. *Int. J. Refract. Met. Hard Mater.* **2008**, *26*, 491–498. [CrossRef]
19. Fernandes, C.M.; Senos, A.M.R.; Vieira, M.T. Versatility of the sputtering technique in the processing of WC-Fe-Ni-Cr composites. *Surf. Coat. Tech.* **2012**, *206*, 4915–4921. [CrossRef]
20. Chang, S.H.; Chang, M.H.; Huang, K.T. Study on the sintered characteristics and properties of nanostructured WC-15 wt% (Fe-Ni-Co) and WC-15 wt% Co hard metal alloys. *J. Alloys Compd.* **2015**, *649*, 89–95. [CrossRef]
21. Reichel, B.; Wagner, K.; Janisch, D.S.; Lengauer, W. Alloyed W-(Co,Ni,Fe)-C phases for reaction sintering of hardmetals. *Int. J. Refract. Met. Hard Mater.* **2010**, *28*, 638–645. [CrossRef]
22. Zhao, Z.Y.; Liu, J.W.; Tang, H.G.; Ma, X.F.; Zhao, W. Investigation on the mechanical properties of WC-Fe-Cu hard alloys. *J. Alloys Compd.* **2015**, *632*, 729–734. [CrossRef]
23. Razavi, M.; Rahimipour, M.R.; Yazdani-Rad, R. Synthesis of Fe-WC nanocomposite from industrial ferrotungsten via mechanical alloying method. *Adv. Appl. Ceram.* **2011**, *110*, 367–374. [CrossRef]
24. Shon, I.J. Rapid consolidation of nanostructured WC-FeAl hard composites by high-frequency induction heating and its mechanical properties. *Int. J. Refract. Met. Hard Mater.* **2016**, *61*, 185–191. [CrossRef]
25. Mosbah, A.Y.; Wexler, D.; Calka, A. Tungsten carbide iron aluminide hardmetals: Nanocrystalline vs. microcrystalline. *J. Metastable Nanocryst. Mater.* **2001**, *10*, 649–654. [CrossRef]
26. Furushima, R.; Katou, K.; Shimojima, K.; Hosokawa, H.; Matsumoto, A. Control of WC grain sizes and mechanical properties in WC-FeAl composite fabricated from vacuum sintering technique. *Int. J. Refract. Met. Hard Mater.* **2015**, *50*, 16–22. [CrossRef]
27. Huang, S.G.; Van der Biest, O.; Vleugels, J. Pulsed electric current sintered Fe_3Al bonded WC composites. *Int. J. Refract. Met. Hard Mater.* **2009**, *27*, 1019–1023. [CrossRef]
28. Hanyaloglu, C.; Aksakal, B.; Bolton, J.D. Production and indentation analysis of WC/Fe-Mn as an alternative to cobalt-bonded hardmetals. *Mater. Charact.* **2001**, *47*, 315–322. [CrossRef]
29. Maccio, M.R.; Berns, H. Sintered hardmetals with iron-manganese binder. *Powder Metall.* **2012**, *55*, 101–109. [CrossRef]
30. Qian, C.; Kun, L.I.; Guo, X.; Liu, B.; Long, Z.; Liu, Y. Effect of WC grain size on mechanical properties and microstructures of cemented carbide with medium entropy alloy Co-Ni-Fe binder. *J. Cent. South Univ.* **2020**, *27*, 1146–1157. [CrossRef]
31. Machado, I.F.; Girardini, L.; Lonardelli, I.; Molinari, A. The study of ternary carbides formation during SPS consolidation process in the WC-Co-steel system. *Int. J. Refract. Met. Hard Mater.* **2009**, *27*, 883–891. [CrossRef]
32. Oliveira, A.B.; Bastos, A.C.; Fernandes, C.M.; Pinho, C.M.S.; Senos, A.M.R.; Soares, E.; Sacramento, J.; Zheludkevich, M.L.; Ferreira, M.G.S. Corrosion behaviour of WC-10% AISI 304 cemented carbides. *Corros. Sci.* **2015**, *100*, 322–331. [CrossRef]
33. Fernandes, C.M.; Senos, A.M.R.; Vieira, M.T. Sintering of tungsten carbide particles sputter-deposited with stainless steel. *Int. J. Refract. Met. Hard Mater.* **2003**, *21*, 147–154. [CrossRef]
34. Fernandes, C.M.; Senos, A.M.R.; Vieira, M.T. Microscopic characterization of the thermal evolution of stainless steel coatings sputter-deposited onto WC particles. *Microsc. Microanal.* **2008**, *14*, 39–40. [CrossRef]
35. Fernandes, C.M.; Vilhena, L.M.; Pinho, C.M.S.; Oliveira, F.J.; Soares, E.; Sacramento, J.; Senos, A.M.R. Mechanical characterization of WC-10 wt% AISI 304 cemented carbides. *Mater. Sci. Eng. A* **2014**, *618*, 629–636. [CrossRef]
36. Lou, D.; Hellman, J.; Luhulima, D.; Liimatainen, J.; Lindroos, V.K. Interactions between tungsten carbide (WC) particulates and metal matrix in WC-reinforced composites. *Mater. Sci. Eng. A* **2003**, *340*, 155–162. [CrossRef]
37. Bounhoure, V.; Lay, S.; Coindeau, S.; Norgren, S.; Pauty, E.; Missiaen, J.M. Effect of Cr addition on solid state sintering of WC-Co alloys. *Int. J. Refract. Met. Hard Mater.* **2015**, *52*, 21–28. [CrossRef]
38. Huang, Z.; Ren, X.R.; Liu, M.X.; Xu, C.; Zhang, X.H.; Guo, S.D.; Chen, H. Effect of Cu on the microstructures and properties of WC-6Co cemented carbides fabricated by SPS. *Int. J. Refract. Met. Hard Mater.* **2017**, *62*, 155–160. [CrossRef]
39. Lin, N.; Jiang, Y.; Zhang, D.F.; Wu, C.H.; He, Y.H.; Xiao, D.H. Effect of Cu, Ni on the property and microstructure of ultrafine WC-10Co alloys by sinter-hipping. *Int. J. Refract. Met. Hard Mater.* **2011**, *29*, 509–515. [CrossRef]

40. Arenas, F.J.; Matos, A.; Cabezas, M.; Di Rauso, C.; Grigorescu, C. Densification, mechanical properties and wear behavior of WC-VC-Co-Al hardmetals. *Int. J. Refract. Met. Hard Mater.* **2001**, *19*, 381–387. [CrossRef]
41. Kim, J.; Suh, Y.J.; Kang, L. First-principles calculations of the phase stability and the elastic and mechanical properties of eta-phases in the WC-Co system. *J. Alloys Compd.* **2016**, *656*, 213–217. [CrossRef]
42. Ren, X.Y.; Peng, Z.J.; Wang, C.B.; Fu, Z.Q.; Qi, L.H.; Miao, H.Z. Effect of ZrC nanopowder addition on the microstructure and mechanical properties of binderless tungsten carbide fabricated by spark plasma sintering. *Int. J. Refract. Met. Hard Mater.* **2015**, *48*, 398–407. [CrossRef]
43. Jiang, Y.; Yang, J.F.; Fang, Q.F. Effect of chromium content on microstructure and corrosion behavior of W-Cr-C coatings prepared on tungsten substrate. *Front. Mater. Sci.* **2015**, *9*, 77–84. [CrossRef]
44. Silva, V.L.; Fernandes, C.M.; Senos, A.M.R. Copper wettability on tungsten carbide surfaces. *Ceram. Int.* **2016**, *42*, 1191–1196. [CrossRef]
45. Ray, N.; Kempf, B.; Mutzel, T.; Heringhaus, F.; Froyen, L.; Vanmeensel, K.; Vleugels, J. Effect of Ni addition on the contact resistance of Ag-WC electrical contacts. *J. Alloys Compd.* **2016**, *670*, 188–197. [CrossRef]
46. Puga, J.B.; Fernandes, C.M.; Vieira, M.T.; Senos, A.M.R. Morphological characterization by scanning electron microscopy of WC powder particles coated with Cu. *Microsc. Microanal.* **2013**, *19*, 145–146. [CrossRef]
47. Chen, C.S.; Yang, C.C.; Chai, H.Y.; Yeh, J.W.; Chau, J.L.H. Novel cermet material of WC/multi-element alloy. *Int. J. Refract. Met. Hard Mater.* **2014**, *43*, 200–204. [CrossRef]
48. Shon, I.J. Effect of Al on sintering and mechanical properties of WC-Al composites. *Ceram. Int.* **2016**, *42*, 17884–17891. [CrossRef]
49. Konyashin, I.; Lachmann, F.; Ries, B.; Mazilkin, A.A.; Straumal, B.B.; Kübel, C.; Llanes, L.; Baretzky, B. Strengthening zones in the Co matrix of WC–Co cemented carbides. *Scripta Mater.* **2014**, *83*, 17–20. [CrossRef]
50. Lindera, D.; Holmström, E.; Norgren, S. High entropy alloy binders in gradient sintered hardmetal. *Int. J. Refr. Met. Hard Mater.* **2018**, *71*, 217–220. [CrossRef]
51. Zhou, P.-F.; Xiao, D.-H.; Yuan, T.-C. Comparison between ultrafinegrained WC–Co and WC–HEA-cemented carbides. *Powder Metall.* **2017**, *60*, 1–6. [CrossRef]
52. Zhou, P.L.; Xiao, D.H.; Zhou, P.F.; Yuan, T.C. Microstructure and properties of ultrafine grained AlCrFeCoNi/WC cemented carbides. *Ceram. Intern.* **2018**, *44*, 17160–17166. [CrossRef]
53. Luo, W.; Liu, Y.; Shen, J. Effects of binders on the microstructures and mechanical properties of ultrafineWC-10%Al_xCoCrCuFeNi composites by spark plasma sintering. *J. Alloys Compd.* **2019**, *791*, 540–549. [CrossRef]
54. Chen, R.; Zheng, S.; Zhou, R.; Wei, B.; Yang, G.; Chen, P.; Cheng, J. Development of cemented carbides with CoxFeNiCrCu high-entropy alloyed binder prepared by spark plasma sintering. *Int. J. Refr. Met. Hard Mater.* **2022**, *103*, 105751. [CrossRef]
55. De Oro Calderon, R.; Edtmaier, C.; Schubert, W.-D. Novel binders for WC-based cemented carbides with high Cr contents. *Int. J. Refr. Met. Hard Mater.* **2019**, *85*, 105063. [CrossRef]
56. Dong, D.; Xiang, X.; Huang, B.; Xiong, H.; Zhang, L.; Shi, K.; Liao, J. Microstructure and properties of WC-Co/CrMnFeCoNi composite cemented carbides. *Vacuum* **2020**, *179*, 109571. [CrossRef]
57. Velo, I.L.; Gotor, F.J.; Alcalá, M.D.; Real, C.; Córdoba, J.M. Fabrication and characterization of WC-HEA cemented carbide based on the CoCrFeNiMn high entropy alloy. *J. Alloys Compd.* **2018**, *746*, 1–8. [CrossRef]
58. Holmström, E.; Lizárrag, R.; Linder, D.; Salmasi, A.; Wang, W.; Kaplan, B.; Mao, H.; Larsson, H.; Vitos, L. High entropy alloys: Substituting for cobalt in cutting edge technology. *Appl. Mater. Today* **2018**, *12*, 322–329. [CrossRef]
59. Pittari III, J.J.; Murdoch, H.A.; Kilczewski, S.M.; Hornbuckle, B.C.; Swab, J.J.; Darling, K.A.; Wright, J.C. Sintering of tungsten carbide cermets with an iron-based ternary alloy binder: Processing and thermodynamic considerations. *Int. J. Refr. Met. Hard Mater.* **2018**, *76*, 1–11. [CrossRef]
60. Ryzhkin, A.A.; Burlakova, V.E.; Moiseev, D.V.; Puchkin, V.N.; Fominoff, E.V. Determination of the efficiency of high entropy cutting tool materials. *J. Frict. Wear* **2016**, *37*, 47–54. [CrossRef]
61. Mueller-Grunz, A.; Alveen, P.; Rassbach, S.; Useldinger, R.; Moseley, S. The manufacture and characterization of WC-(Al)CoCrCuFeNi cemented carbides with nominally high entropy alloy binders. *Int. J. Refr. Met. Hard Mater.* **2019**, *84*, 105032. [CrossRef]
62. Qian, C.; Liu, Y.; Cheng, H.; Li, K.; Liu, B. Effect of the carbon content on the morphology evolution of the η phase in cemented carbides with the CoNiFeCr high entropy alloy binder. *Int. J. Refr. Met. Hard Mater.* **2022**, *102*, 105731. [CrossRef]
63. Luo, W.; Liu, Y.; Liu, X.; Zhou, Z. Oxidation behavior of ultrafine WC-based cemented carbides with Al_xCoCrCuFeNi high-entropy alloy binders. *Ceram. Intern.* **2021**, *47*, 8498–8509. [CrossRef]
64. Li, C.-W.; Chang, K.-C.; Yeh, A.-C. On the microstructure and properties of an advanced cemented carbide system processed by selective laser melting. *J. Alloys Compd.* **2019**, *782*, 440–450. [CrossRef]
65. Li, X.; Wei, D.; Vitos, L.; Lizárrag, R. Micro-mechanical properties of new alternative binders for cemented carbides: CoCrFeNiW_x high-entropy alloys. *J. Alloys Compd.* **2020**, *820*, 153141. [CrossRef]
66. Bratberg, J.; Jansson, B. Thermodynamic evaluation of the C–Co–W–Hf–Zr system for cemented carbides. *JPEDAV* **2006**, *27*, 213–219. [CrossRef]
67. Yadav, S.; Zhang, Q.; Behera, A.; Haridas, R.S.; Agrawal, P.; Gong, J.; Mishra, R.S. Role of binder phase on the microstructure and mechanical properties of a mechanically alloyed and spark plasma sintered WC-FCC HEA composites. *J. Alloys Compd.* **2021**, *877*, 160265. [CrossRef]

68. De la Obra, A.G.; Sayagués, M.J.; Chicardi, E.; Gotor, F.J. Development of Ti(C,N)-based cermets with (Co,Fe,Ni)-based high entropy alloys as binder phase. *J. Alloys Compd.* **2020**, *814*, 152218. [CrossRef]
69. Luo, W.; Liu, Y.; Luo, Y.; Wu, M. Fabrication and characterization of WC-AlCoCrCuFeNi high-entropy alloy composites by spark plasma sintering. *J. Alloys Compd.* **2018**, *754*, 163–170. [CrossRef]
70. Qian, C.; Li, K.; Cheng, H.; Zhang, W.; Jiang, X.; Liu, Y. Fracture behavior of cemented carbides with CoNiFe medium entropy alloy binder. *Int. J. Refr. Met. Hard Mater.* **2021**, *98*, 105547. [CrossRef]
71. Suetin, D.V.; Medvedeva, N.I. Structural, electronic and magnetic properties of carbides M_3W_3C(M = Ti, V, Cr, Mn, Fe, Co, Ni). *J. Alloy. Compd.* **2016**, *681*, 508–515. [CrossRef]
72. Konyashin, I.; Straumal, B.B.; Ries, B.; Bulatov, M.F.; Kolesnikova, K.I. Contact angles of WC/WC grain boundaries with binder in cemented carbides with various carbon content. *Mater. Lett.* **2017**, *196*, 1–3. [CrossRef]
73. Konyashin, I.; Ries, B.; Hlawatschek, D.; Zhuk, Y.; Mazilkin, A.; Straumal, B.; Dorn, F.; Park, D. Wear-resistance and hardness: Are they directly related for nanostructured hard materials? *Int. J. Refract. Met. Hard Mater.* **2015**, *49*, 203–211. [CrossRef]
74. Straumal, B.B.; Semenov, V.N.; Kogtenkova, O.A.; Watanabe, T. Pokrovsky-Talapov critical behavior and rough-to-rough ridges of the ∑3 coincidence tilt boundary in Mo. *Phys. Rev. Lett.* **2004**, *92*, 196101. [CrossRef]
75. Straumal, B.B.; Kogtenkova, O.A.; Gornakova, A.S.; Sursaeva, V.G.; Baretzky, B. Review: Grain boundary faceting-roughening phenomena. *J. Mater. Sci.* **2016**, *51*, 382–404. [CrossRef]
76. Ernst, F.; Finnis, M.W.; Koch, A.; Schmidt, C.; Straumal, B.; Gust, W. Structure and energy of twin boundaries in copper. *Z. Metallk.* **1996**, *87*, 911–922.
77. Protasova, S.G.; Kogtenkova, O.A.; Straumal, B.B. Faceting of individual ∑3 Grain boundaries in Al. *Mater. Sci. Forum* **2007**, *558–559*, 949–954. [CrossRef]
78. Straumal, B.B.; Polyakov, S.A.; Bischoff, E.; Gust, W.; Mittemeijer, E.J. Faceting of Σ3 and Σ9 grain boundaries in copper. *Interface Sci* **2001**, *9*, 287–292. [CrossRef]
79. Sursaeva, V.G.; Straumal, B.B.; Gornakova, A.S.; Shvindlerman, L.S.; Gottstein, G. Effect of faceting on grain boundary motion in Zn. *Acta Mater.* **2008**, *56*, 2728–2734. [CrossRef]
80. Straumal, B.B.; Polyakov, S.A.; Bischoff, E.; Gust, W.; Baretzky, B. Faceting of ∑3 and ∑9 grain boundaries in Cu–Bi alloys. *Acta Mater.* **2005**, *53*, 247–254. [CrossRef]
81. Straumal, B.B.; Konyashin, I.; Ries, B.; Straumal, A.B.; Mazilkin, A.A.; Kolesnikova, K.I.; Gusak, A.M.; Baretzky, B. Pseudopartial wetting of WC/WC grain boundaries in cemented carbides. *Mater. Lett.* **2015**, *147*, 105–108. [CrossRef]
82. Straumal, B.B.; Korneva, A.; Kuzmin, A.; Lopez, G.; Rabkin, E.; Straumal, A.B.; Gerstein, G.; Gornakova, A.S. The grain boundary wetting phenomena in the Ti-containing high entropy alloys: A review. *Metals* **2021**, *11*, 1881. [CrossRef]
83. Straumal, B.B.; Korneva, A.; Lopez, G.A.; Kuzmin, A.; Rabkin, E.; Gerstein, G.; Straumal, A.B.; Gornakova, A.S. Grain boundary wetting by a second solid phase in the high entropy alloys: A review. *Materials* **2021**, *14*, 7506. [CrossRef]
84. Straumal, B.B.; Kulagin, R.; Baretzky, B.; Anisimova, N.Y.; Kiselevskiy, M.V.; Klinger, L.; Straumal, P.B.; Kogtenkova, O.A.; Valiev, R.Z. Severe plastic deformation and phase transformations in high entropy alloys: A review. *Crystals* **2022**, *12*, 54. [CrossRef]